

## Rare earth element (REE) lanthanum substituted MnFe<sub>2</sub>O<sub>4</sub> nanoparticles for photocatalytic and magneto-optical properties

G. Valarmathi<sup>1,\*</sup>, G. Mathubala<sup>1</sup>

<sup>1</sup> Department of Chemistry,

Bharath Institute of Higher Education and Research (BIHER),

Bharath University, Chennai, 600073, Tamil Nadu, India

\*Corresponding author Email: [elamathielango234@gmail.com](mailto:elamathielango234@gmail.com) (G. Valarmathi).

### Address for Correspondence

G. Valarmathi<sup>1,\*</sup>, G. Mathubala<sup>1</sup>

<sup>1</sup> Department of Chemistry,

Bharath Institute of Higher Education and Research (BIHER),

Bharath University, Chennai, 600073, Tamil Nadu, India

\*Corresponding author Email: [elamathielango234@gmail.com](mailto:elamathielango234@gmail.com) (G. Valarmathi).

### Abstract

Nanocrystalline spinel MnLa<sub>x</sub>Fe<sub>2-x</sub>O<sub>4</sub> ( $0 \leq x \leq 0.5$ ) was synthesized by microwave combustion technique (MCT) utilizing the fuel *urea*. The establishment of cubic spinel is ensured by powder X-ray diffraction (PXRD) and the crystal size was found to exist in the range of 27.52 to 13.12 nm for spinel MnLa<sub>x</sub>Fe<sub>2-x</sub>O<sub>4</sub> ( $0 \leq x \leq 0.5$ ) nanoparticles (NPs). Further morphology of the MnLa<sub>x</sub>Fe<sub>2-x</sub>O<sub>4</sub> NPs was observed by high resolution scanning electron microscope (HR-SEM). Energy dispersive X-ray (EDX) studies confirmed the formation pure spinel ferrite structure as it ensured the presence of all the elements. The appearance of Fourier transform infra-red (FT-IR) band at 420, 450 cm<sup>-1</sup>, is linked to octahedral-metal stretching (Ni-O) and band at 575 cm<sup>-1</sup>, is linked to the tetrahedral metal stretching (Fe-O), which ensures the formation spinel MnLa<sub>x</sub>Fe<sub>2-x</sub>O<sub>4</sub> ( $0 \leq x \leq 0.5$ ) nanoparticles. Finally, the magnetic properties such as Mr, Hc and Ms were calculated from the M-H loops which exhibited ferromagnetic behaviour.

**Keywords:** La substituted MnFe<sub>2</sub>O<sub>4</sub> NPs; Optical properties; Magnetic properties.

### 1. Introduction

The cubic spinel structure general formula of AB<sub>2</sub>O<sub>4</sub>, (where: A<sup>2+</sup>= Co<sup>2+</sup>, Zn<sup>2+</sup>, Mn<sup>2+</sup>, Ni<sup>2+</sup>, etc.) divalent metal ion occupy the tetrahedral (A) sites and (where: B<sup>3+</sup>= Fe<sup>3+</sup>, Al<sup>3+</sup>, etc.)

octahedral (B) site is occupied by trivalent metal ion [1-6]. It is observed that these ferrites exhibited distinct magnetic and physical characteristics upon alteration of the divalent cation.

By altering, the divalent cation, it is feasible to obtain expressively different magnetic and physical characteristics in ferrites. Previous study conveys Ce-Ni ferrites exhibit unique characteristics and proved to be a versatile magnetic material widely used in power transformers, microwave devices, read/write heads for high speed digital tape power transformers, rod antennas [7], and gas sensing material [8-10].

The techniques such as sol-gel, solvothermal, microwave assisted combustion method, co-precipitation, ball milling method and hydrothermal are widely used to synthesize cerium substituted nickel ferrite nanoparticles [11-15]. However, above stated methods are found to be expensive, difficult to synthesis, high cost, time consuming and yield was low. In addition, the microwave combustion method is used to synthesize cerium doped nickel ferrite nanoparticles by this report [16-20]. In this technique there is an abrupt increase in the temperature of the precursor due to the intrinsic nature of microwave energy which generates heat and conversion by virtue of its strong inter molecular friction.

## 2. Experimental

### 2.1. Synthesis

Spinel  $\text{MnLa}_x\text{Fe}_{2-x}\text{O}_4$  ( $0 \leq x \leq 0.5$ ) nanoparticles were synthesized using the corresponding metal nitrates  $\text{Mn}(\text{NO}_3)_2 \cdot 6\text{H}_2\text{O}$ ,  $\text{La}(\text{NO}_3)_3 \cdot 6\text{H}_2\text{O}$ ,  $\text{Fe}(\text{NO}_3)_3 \cdot 9\text{H}_2\text{O}$  and the fuel urea. The chemicals were brought from SD fine, India that was of analytical grade and utilized as it is deprived of additional purification. In order to prepare the samples double distilled water was employed.  $\text{Mn}(\text{NO}_3)_2 \cdot 6\text{H}_2\text{O}$ ,  $\text{La}(\text{NO}_3)_3 \cdot 6\text{H}_2\text{O}$  and  $\text{Fe}(\text{NO}_3)_3 \cdot 9\text{H}_2\text{O}$  serves as precursors which were mixed distinctly to determine homogeneous solutions, by maintaining a molar ratio of 1:2. The attained solutions were added with plant extracts of *urea*, which was further mixed for 1 hour. Here, plant extracts of *urea* is employed as fuel while nitrates precursor serves as oxidizers.

The final obtained homogeneous solutions were transferred into two silica crucibles. The silica crucibles were placed in domestic microwave ovens obtained from SAMSUNG, India utilized for the mechanism of irradiation. The output power was set in both the microwave ovens for 10 min at 900 Watts and frequency was maintained at 2.54 GHz. Under the influence of microwave energy, the solutions underwent the process like boiling, vaporizing, dehydration and

finally decomposition resulting in evolution of reaction gas. When the solutions attained the spontaneous combustion, ignition took place, which causes rapid flame fluffy production of pure spinel  $\text{MnLa}_x\text{Fe}_{2-x}\text{O}_4$  ( $0 \leq x \leq 0.5$ ) nanoparticles. Further, the obtained samples were washed with distilled water, ethanol and dried at  $550^\circ\text{C}$  for 150 min.

## 2.2. Characterization techniques

X-ray powder diffractometer is employed to confirm the formation of phase and investigate the crystal structure of the obtained spinel  $\text{MnLa}_x\text{Fe}_{2-x}\text{O}_4$  ( $0 \leq x \leq 0.5$ ) nanoparticles employing  $\text{CuK}\alpha$  radiation at  $\lambda = 1.5406 \text{ \AA}$  radiation by varying  $2\theta$  range from  $20^\circ$  to  $80^\circ$  (Model Rigaku Ultima III). FEI Quanta FEG 200 scanning electron microscope accompanied with energy dispersive X-ray analyser is utilized to perform morphological and elemental analysis. The diffuse reflectance spectrum was logged utilizing Perkin Elmer (Thermo Scientific Evolution 220) spectrophotometer from which the band gap value is deduced by operating it in the range of 200-800 nm. Perkin Elmer spectrophotometer (Spectrum RX1) is utilized to log the FTIR spectrum. Lake Shore, USA, Model7404 equipped with 3 magnets is used to perform Vibration sample magnetometry at RT.

## 3. Results and discussion

### 3.1. Phase analysis

The XRD pattern of the as prepared spinel  $\text{MnLa}_x\text{Fe}_{2-x}\text{O}_4$  nanoparticles is illustrated in Fig. 1. From the attained powder patterns it is confirmed that the prepared samples were polycrystalline in nature [16-20]. The peaks at  $2\theta$  values of  $18.24^\circ$ ,  $37.20^\circ$ ,  $43.23^\circ$ ,  $54.03^\circ$ ,  $62.92^\circ$  and  $75.35^\circ$  are mapped to (111), (220), (311), (222), (400), (440) and (622) reflection planes of spinel  $\text{MnLa}_x\text{Fe}_{2-x}\text{O}_4$  ( $0 \leq x \leq 0.5$ ) nanoparticles. The attained diffraction peaks go with diffraction data (JCPDS card number 44-1485) ensuring the establishment of cubic spinel structure with  $Fd\text{-}3m$  space group [21-25]. All the samples impurity peaks were associated with the  $\alpha\text{-Fe}_2\text{O}_3$  phase verified by the card ICSD – 08842 data. This impurity phase may be due to the oxidation ability of  $\text{Ni}^{2+}$  ion and the combustion in oxygen rich environment [25].

The average crystallite ( $L$ ) of the obtained nanoparticles estimated using (311) reflection plane by employing Debye Scherrer's Eq. (1).

$$L = \frac{0.89 \lambda}{\beta \cos \theta} \quad (1)$$

Where,  $L$ , is the average crystallite size;  $\lambda$ , the X-ray source wavelength (0.15406 nm);  $\beta$ , the full width at half maximum (FWHM) of the observed diffraction peak; and  $\theta$ , the diffraction angle. The value of the average crystallite size deduced for spinel  $MnLa_xFe_{2-x}O_4$  ( $0 \leq x \leq 0.5$ ) nanoparticles corresponding to the diffraction peak (311) were established to be lie within 15 to 25 nm respectively.

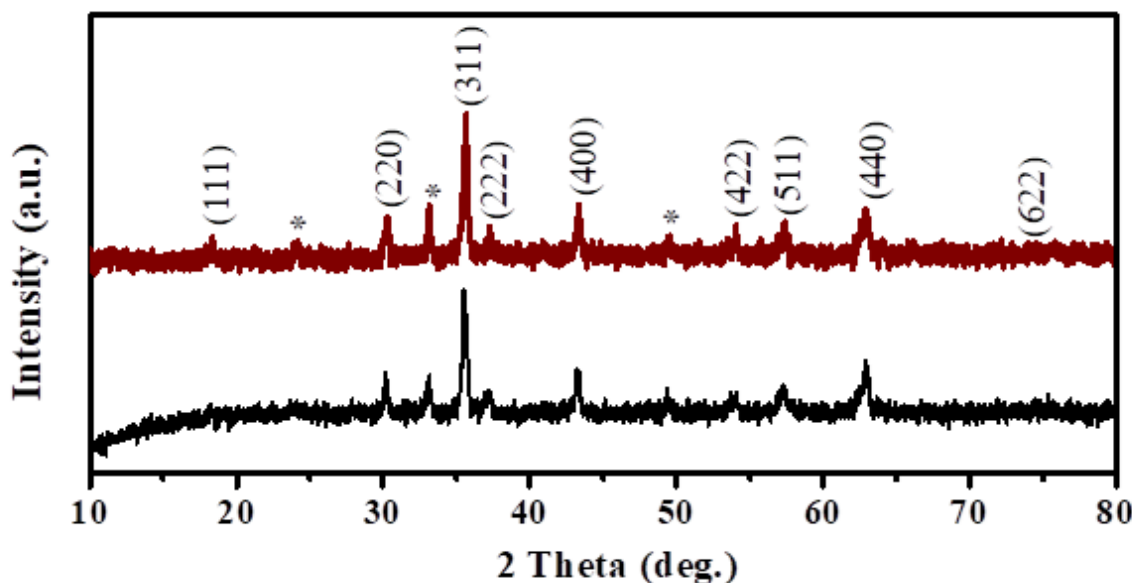


**Fig. 1. Powder XRD patterns of spinel  $MnLa_xFe_{2-x}O_4$  ( $0 \leq x \leq 0.5$ ) nanoparticles.**

In order to deduce the lattice parameter of the spinel  $MnLa_xFe_{2-x}O_4$  ( $0 \leq x \leq 0.5$ ) nanoparticles using Eq. 2 as follows:

$$a = d_{hkl} \sqrt{(h^2 + k^2 + l^2)} \quad (2)$$

Where,  $d_{hkl}$ , the inter-atomic spacing corresponding to the miller indices;  $h$ ,  $k$ , and  $l$  of the crystal planes and  $a$ , is the lattice parameter. This increase in lattice parameter is due to the substitution of larger ionic size Ce cations (0.92 Å) in place of the lower ionic size Fe cations (0.67 Å) [3].

### 3.2 SEM analysis

Spinel  $MnLa_xFe_{2-x}O_4$  ( $0 \leq x \leq 0.5$ ) nanoparticles morphology study is performed with aid of HR-SEM. The obtained SEM images of spinel  $MnLa_xFe_{2-x}O_4$  ( $0 \leq x \leq 0.5$ ) nanoparticles illustrated a spherical morphology beside it reveal coalescence and agglomerated shown in Fig. 5. The

agglomerated and spherical morphology was noticed in the spinel  $\text{MnLa}_x\text{Fe}_{2-x}\text{O}_4$  ( $0 \leq x \leq 0.5$ ) nanoparticles, which is mainly due to the lower energy during the process of combustion [28].

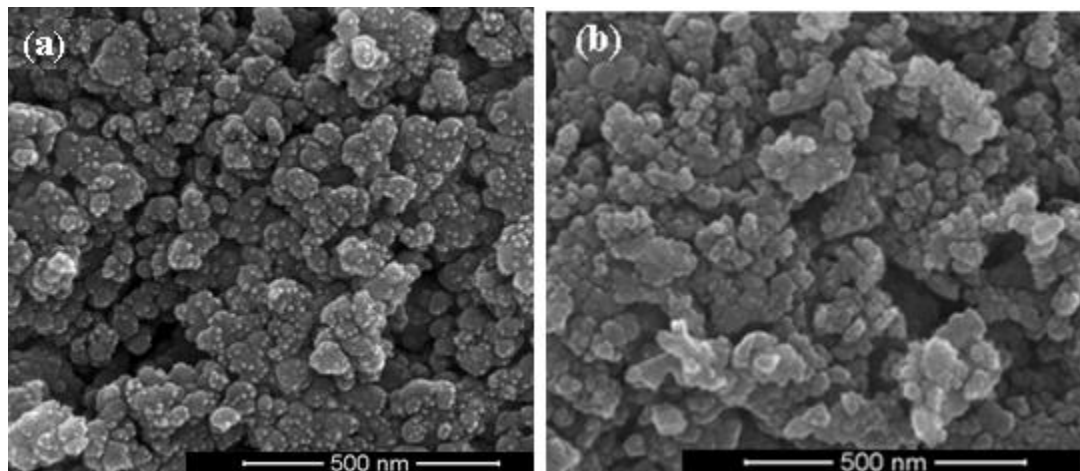


**Fig. 2. SEM images of spinel  $\text{MnLa}_x\text{Fe}_{2-x}\text{O}_4$  ( $0 \leq x \leq 0.5$ ) nanoparticles.**

### 3.3 HR-TEM analysis

To obtain further information on the nano-scaled fine structure of spinel  $\text{MnLa}_x\text{Fe}_{2-x}\text{O}_4$  ( $0 \leq x \leq 0.5$ ) nanoparticles, a structural analysis of the particles was performed by high resolution transmission electron microscopy (HR-TEM) and is revealed in Fig. 3. The HR-TEM images of the samples clearly show that spherical shaped particles like nanostructures. Crystallographic clarifications of the as prepared sample was done by recording the selected area electron diffraction (SAED) patterns of spinel  $\text{MnLa}_x\text{Fe}_{2-x}\text{O}_4$  ( $0 \leq x \leq 0.5$ ) nanoparticles.

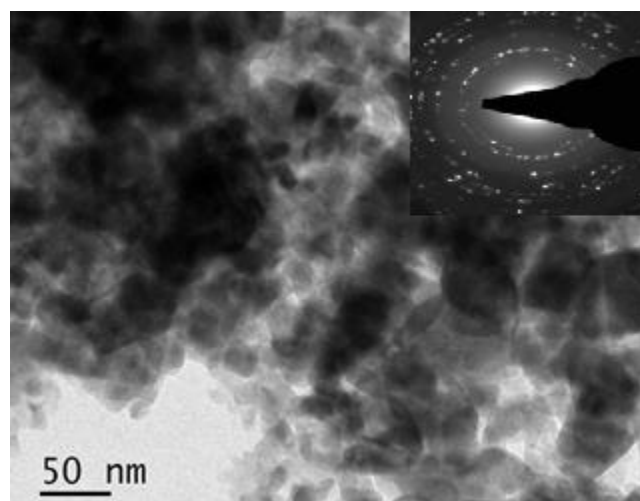


**Fig. 3. TEM images of spinel  $\text{MnLa}_x\text{Fe}_{2-x}\text{O}_4$  ( $0 \leq x \leq 0.5$ ) nanoparticles.**

### 3.4. Optical band gap analysis

In order to study the optical and band gap characteristics of spinel  $\text{MnLa}_x\text{Fe}_{2-x}\text{O}_4$  ( $0 \leq x \leq 0.5$ ) nanoparticles UV-visible diffuse reflectance spectroscopy (UV-Vis DRS) is used, which determined bandgap with aid of Tauc relation. Kubelka-Munk function  $F(R)$  is utilized to transform the diffused reflectance into absorption co-efficient, as stated in equation (4).

$$\alpha = F(R) = \frac{(1-R)^2}{2R} \quad (4)$$

Where,  $\alpha$  is the absorption coefficient and  $R$  is reflectance. Thus, the Tauc relation can be stated in equation (5),

$$F(R)hv = A(hv - E_g)^n \quad (5)$$

Where  $A$ ,  $v$ ,  $h$ , and  $E_g$ , absorption coefficient, light frequency, Plank's constant and band gap respectively. The permitted direct and indirect transitions are denoted by  $n = 2$  and  $1/2$ , from where the values of the both direct as well as indirect bandgap is obtained.

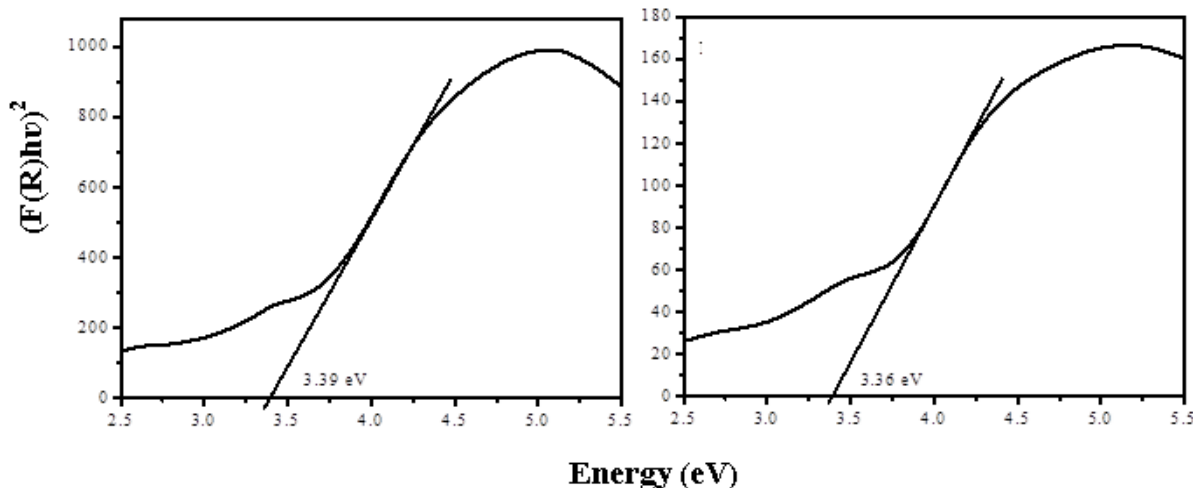


**Fig. 4. Band gap of spinel  $\text{MnLa}_x\text{Fe}_{2-x}\text{O}_4$  ( $0 \leq x \leq 0.5$ ) nanoparticles.**

### 3.5 FT-IR analysis

FT-IR spectrum of spinel  $\text{MnLa}_x\text{Fe}_{2-x}\text{O}_4$  ( $0 \leq x \leq 0.5$ ) nanoparticles is depicted in Fig. 5. The FT-IR spectrum was recorded in the range of  $4000-400 \text{ cm}^{-1}$  at room temperature (RT). The broad band at  $3440 \text{ cm}^{-1}$  are linked to H-O stretching [21-25]. The C-H stretching vibration is associated with the band at  $2926$  and  $2851 \text{ cm}^{-1}$  [26]. The characteristic absorption bands at

1400-1750 cm<sup>-1</sup> are assigned to C-O stretching vibration due to the presence of traces of organic species (e.g. COO<sup>-</sup>) on the particle surface [27-30]. The bands in between, 1000-1220 cm<sup>-1</sup> are associated with vibration of due to spinel structure of NiFe<sub>2</sub>O<sub>4</sub> NPs respectively [31]. The band at 420-450 cm<sup>-1</sup>, is assigned to octahedral-metal stretching (Ni-O) and 575 cm<sup>-1</sup>, is linked to the tetrahedral metal stretching (Fe-O) [32].

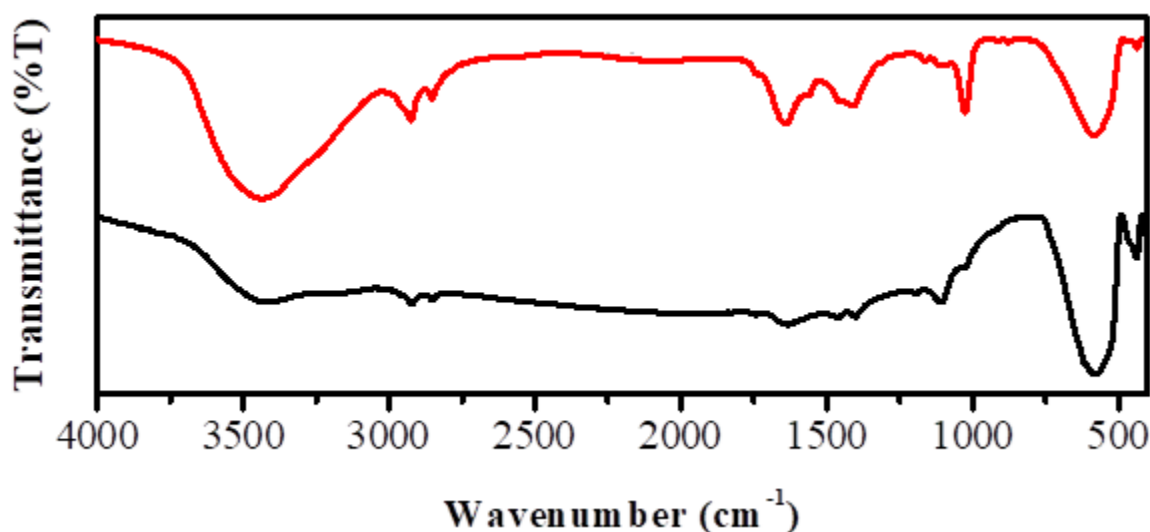


**Fig. 5. FT-IR spectra of spinel MnLa<sub>x</sub>Fe<sub>2-x</sub>O<sub>4</sub> ( $0 \leq x \leq 0.5$ ) nanoparticles.**

### 3.6. Magnetization analysis

The magnetic properties of the spinel MnLa<sub>x</sub>Fe<sub>2-x</sub>O<sub>4</sub> ( $0 \leq x \leq 0.5$ ) nanoparticles were undertaken at temperature of 300 K and stimulated magnetic field is found to lie in the range -15 kOe to +15kOe. Magnetization (M) versus applied field (H) behavior plots are shown in Fig. 9. From the hysteresis (M-H) loop coercivity (H<sub>c</sub>), remanence magnetization (M<sub>r</sub>) and saturation magnetization (M<sub>s</sub>) were determined. Spinel MnLa<sub>x</sub>Fe<sub>2-x</sub>O<sub>4</sub> ( $0 \leq x \leq 0.5$ ) nanoparticles exhibited normal spinel structure, as divalent (Ni<sup>2+</sup>) and trivalent (Ce<sup>3+</sup>/Fe<sup>3+</sup>) metal ions resides in the tetrahedral (A) and octahedral (B) locations [31-35]. The NiFe<sub>2</sub>O<sub>4</sub> NPs were found exhibit ferromagnetic nature. The coercivity values of spinel MnLa<sub>x</sub>Fe<sub>2-x</sub>O<sub>4</sub> ( $0 \leq x \leq 0.5$ ) nanoparticles were found to lie within 292 Oe to 180 Oe (Fig. 10). The coercivity value is mainly controlled by factors such as high anisotropy and cationic redistribution [35-40]. From the M-H hysteresis loop M<sub>r</sub> values for spinel MnLa<sub>x</sub>Fe<sub>2-x</sub>O<sub>4</sub> ( $0 \leq x \leq 0.5$ ) nanoparticles was found to be 7 emu/g for

( $x = 0.0$ ), 7.84 emu/g for ( $x = 0.3$ ) then  $M_r$  values declined to 5.88 emu/g for ( $x = 0.5$ ), whose values are found to be dependent on the crystallite size and shape of  $\text{NiFe}_2\text{O}_4$  [40-42]. From the hysteresis loop  $M_s$  values for spinel  $\text{MnLa}_x\text{Fe}_{2-x}\text{O}_4$  ( $0 \leq x \leq 0.5$ ) nanoparticles was found to be lie within 35 emu/g.

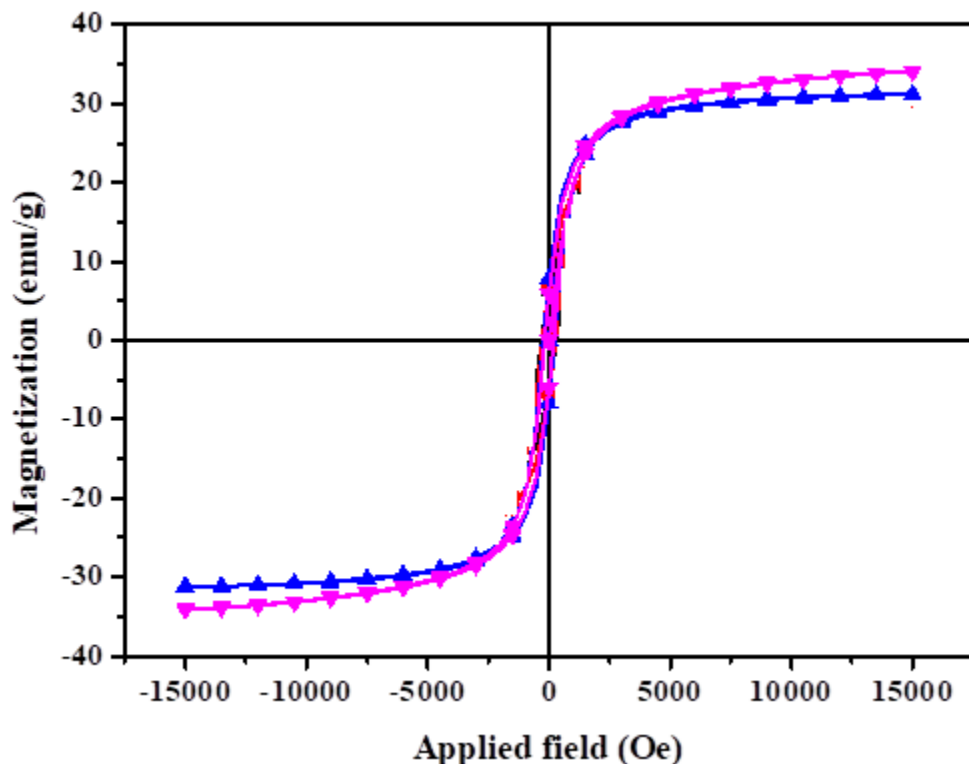


**Fig. 6. VSM studies of spinel  $\text{MnLa}_x\text{Fe}_{2-x}\text{O}_4$  ( $0 \leq x \leq 0.5$ ) nanoparticles.**

#### 4. Conclusions

Spinel  $\text{MnLa}_x\text{Fe}_{2-x}\text{O}_4$  ( $0 \leq x \leq 0.5$ ) nanoparticles were made by MCT, utilizing the fuel urea. The XRD confirmed the cubic spinel structure with  $Fd\text{-}3m$  space group. The lattice parameter values were found to lie within 8.345 Å and 8.395 Å. The surface morphology of the prepared samples is investigated utilizing HR-SEM. EDX analysis confirmed the presence of elements such as Mn, La, Fe and O. The band gap values were observed to be lie within 3.39-3.26 eV attained using the optical absorption spectra. FT-IR unveils the existence of all the characteristic functional groups of spinel  $\text{MnLa}_x\text{Fe}_{2-x}\text{O}_4$  ( $0 \leq x \leq 0.5$ ) nanoparticles.

## References

1. A. P. Subramanian, S. K. Jaganathan, A. Manikandan, K. N. Pandiaraj, N. Gomathi and E. Supriyanto, Recent trends in nano based drug delivery systems for efficient delivery of phytochemicals in chemotherapy, RSC Advances, 6 (2016) 48294-48314.
2. M. A. Almessiere, Y. Slimani, H. Güngüneş, S. Ali, A. Manikandan, I. Ercan, A. Baykal, A.V. Trukhanov, Magnetic Attributes of NiFe<sub>2</sub>O<sub>4</sub> Nanoparticles: Influence of Dysprosium Ions (Dy<sup>3+</sup>) Substitution, Nanomaterials, 9 (2019) 820.
3. V. Muthuvignesh, V.J. Reddy, S. Ramakrishna, S. Ray, A. Ismail, M. Mandal, A. Manikandan, S. Seal and S. K. Jaganathan, Electrospinning applications from diagnosis to treatment of diabetes, RSC Advances, 6 (2016) 83638-83655.
4. V. Muthuvignesh, S. K. Jaganathan, A. Manikandan, Nanomaterials as a game changer in the management and treatment of diabetic foot ulcers, RSC Advances, 6 (2016) 114859-114878.
5. A. Manikandan, A. Saravanan, S. Arul Antony, M. Bououdina, One-pot low temperature synthesis and characterization studies of nanocrystalline α-Fe<sub>2</sub>O<sub>3</sub> based dye sensitized solar cells, Journal of Nanoscience and Nanotechnology, 15 (2015) 4358-4366.
6. S. Asiri, S. Güner, A. Demir, A. Yildiz, A. Manikandan, A. Baykal, Synthesis and Magnetic Characterization of Cu Substituted Barium Hexaferrites, Journal of Inorganic and Organometallic Polymers and Materials, 28 (2018) 1065–1071.
7. D. K. Manimegalai, A. Manikandan, S. Moortheswaran, S. Arul Antony, Magneto-Optical and Photocatalytic Properties of Magnetically Recyclable Zn<sub>1-x</sub>Mn<sub>x</sub>S (x = 0.0, 0.3 and 0.5) nano-catalysts, Journal of Superconductivity and Novel Magnetism, 28 (2015) 2755-2766.
8. P. Thilagavathi, A. Manikandan, S. Sujatha, S. K. Jaganathan, S. Arul Antony, Sol-gel synthesis and characterization studies of NiMoO<sub>4</sub> nanostructures for photocatalytic degradation of methylene blue dye, Nanoscience and Nanotechnology Letters, 8 (2016) 438-443.
9. G. Mathubala, A. Manikandan, S. Arul Antony, P. Ramar, Enhanced photocatalytic activity of spinel Cu<sub>x</sub>Mn<sub>1-x</sub>Fe<sub>2</sub>O<sub>4</sub> nanocatalysts for the degradation of methylene blue dye and opto-magnetic properties, Nanoscience and Nanotechnology Letters, 8 (2016) 375-381.

10. D. Vanitha, B. Sultan Asath, N. Nallaperumal, A. Shunmuganarayanan, A. Manikandan, Electrical Impedance studies on sodium ion conducting composite blend polymer electrolyte, *Journal of Inorganic and Organometallic Polymers and Materials*, 27 (2017) 257–265.
11. K. Geetha, R. Udhayakumar, A. Manikandan, Enhanced magnetic and photocatalytic characteristics of cerium substituted spinel  $MgFe_2O_4$  ferrite nanoparticles, *Physica B: Physics of Condensed Matter*, 615 (2021) 413083, Impact Factor: 2.436. (Elsevier)
12. S. S. Al-Jameel, S. Rehman, M. A. Almessiere, F. A. Khan, Y. Slimani, N. S. Al-Saleh, A. Manikandan, E. A. Al-Suhaimi, A. Baykal, Anti-microbial and anti-cancer activities of  $MnZnDy_xFe_{2-x}O_4$  ( $x \leq 0.1$ ) nanoparticles, *Artificial Cells, Nanomedicine and Biotechnology*, 49 (2021) 493-499.
13. S. Rehman, M. A. Almessiere, S. S. Al-Jameel, U. Ali, Y. Slimani, N. Taskhandi, N. S. Al-Saleh, A. Manikandan, F. A. Khan, E. A. Al-Suhaimi, A. Baykal, Designing of  $Co_{0.5}Ni_{0.5}Ga_xFe_{2-x}O_4$  ( $0.0 \leq x \leq 1.0$ ) Microspheres via Hydrothermal Approach and Their Selective Inhibition on the Growth of Cancerous and Fungal Cells, *Pharmaceutics*, 13 (2021) 962.
14. C. Sambathkumar, R. Ranjithkumar, S. Ezhil Arasi, A. Manikandan, N. Nallamuthu, M. Krishna Kumar, A. Arivarasan, P. Devendran, High-performance nickel sulfide modified electrode material from single source precursor for energy storage application, *Journal of Materials Science: Materials in Electronics*, 32 (2021) 20058-20070.
15. C. Sambathkumar, V. Manirathinam, A. Manikandan, M. Krishna Kumar, S. Sudhakar, P. Devendran, Solvothermal synthesis of  $Bi_2S_3$  nanoparticles for active photocatalytic and energy storage device applications, *Journal of Materials Science: Materials in Electronics*, 32 (2021) 20827-20843.
16. V. S. P. Sakthi Sri, A. Manikandan, M. Mathankumar, R. Tamizhselvi, M. George, A. L. Bilgrami, S. A. Al-Zahrani, A. A. P. Khan, Anish Khan, A. M. Asiri, Unveiling the photosensitive, mechanical and magnetic properties of amorphous iron nanoparticles with its application towards decontamination of water and cancer treatment, *Journal of Materials Research and Technology*, 15 (2021) 99-118.

17. M. A. Almessiere, B. Unal, Y. Slimani, H. Gungunes, M. S. Toprak, N. Tashkand, A. Baykal, M. Sertkol, A.V. Trukhanov, A. Yıldız, A. Manikandan, Effects of Ce-Dy rare earths co-doping on various features of Ni-Co spinel ferrite microspheres prepared via hydrothermal approach, *Journal of Materials Research and Technology*, 14 (2021) 2534-2553.
18. S. Blessi, A. Manikandan, S. Anand, M. M. L. Sonia, V. M. Vinosel, P. Paulraj, Y. Slimani, M.A. Almessiere, M. Iqbal, S. Guner, A. Baykal, Effect of Zinc substitution on the physical and electrochemical properties of mesoporous SnO<sub>2</sub> nanomaterials, *Materials Chemistry and Physics*, 273 (2021) 125122.
19. M. A. Almessiere, Y. Slimani, Y. O. Ibrahim, M. A. Gondal, M. A. Dastageer, I. A. Auwal, A. V. Trukhanov, A. Manikandan, A. Baykal, Morphological, structural, and magnetic characterizations of hard-soft ferrite nanocomposites synthesized via pulsed laser ablation in liquid, *Materials Science and Engineering B*, 273 (2021) 115446.
20. M. A. Almessiere, Y. Slimani, N. A. Algarou, M. A. Gondal, Y. S. Wudil, M. Younas, I. A. Auwal, A. Baykal, A. Manikandan, T. I. Zubari, V. G. Kostishin, A. V. Trukhanov, I. Ercan, Electronic, magnetic, and microwave properties of hard/soft nanocomposites based on hexaferrite SrNi<sub>0.02</sub>Zr<sub>0.02</sub>Fe<sub>11.96</sub>O<sub>19</sub> with variable spinel phase MFe<sub>2</sub>O<sub>4</sub> (M = Mn, Co, Cu, and Zn), *Ceramics International*, 47 (2021) 35209-35223.
21. M. A. Almessiere, Y. Slimani, N. A. Algarou, M. A. Gondal, Y. S. Wudil, M. Younas, I. A. Auwal, A. Baykal, A. Manikandan, Electrospinning synthesis of Cd substituted Ni-Co spinel ferrite nanofibers: An investigation on their structural and magnetic features, *Applied Physics A*, 127 (2021) 785.
22. M. A. Almessiere, Y. Slimani, N. A. Algarou, M. A. Gondal, Y. S. Wudil, M. Younas, I. A. Auwal, A. Baykal, A. Manikandan, Investigation on electrical and dielectric properties of hard/soft spinel ferrite nanocomposites of CoFe<sub>2</sub>O<sub>4</sub>/(NiSc<sub>0.03</sub>Fe<sub>1.97</sub>O<sub>4</sub>)<sub>x</sub>, *Vacuum*, 194 (2021) 110628,
23. N. Kabeerdass, A. Al Otaibi, M. Rajendran, A. Manikandan, H. A. Kashmery, M. M. Rahman, P. Madhu, A. Khan, A. M. Asiri, M. Mathanmohun, Bacillus-Mediated Silver Nanoparticle Synthesis and Its Antagonistic Activity against Bacterial and Fungal Pathogens, *Antibiotics*, 10 (2021) 1334.

24. C. R. T. Kumari, A. Al Otaibi, T. Kamaraj, M. Nageshwari, G. Mathubala, A. Manikandan, M. L. Caroline, S. Sudha, H. A. Kashmery, P. Madhu, A. Khan, H. M. Marwani, A. M. Asiri, A brief study on optical and mechanical properties of an organic material: urea glutaric acid (2/1)-a third order nonlinear optical single crystal, Crystals, 11 (2021) 1239.
25. R. R. Mathiarasu, A. Manikandan, K. Panneerselvam, M. George, Y. Slimani, M. A. Almessiere, A. Baykal, A. M. Asiri, T. Kamal, A. Khan, Photocatalytic degradation of reactive anionic dyes RB5, RR198 and RY145 via Rare earth element (REE) Lanthanum substituted CaTiO<sub>3</sub> perovskite catalysts, Journal of Materials Research and Technology, 15 (2021) 5936-5947.
26. M.A. Almessiere, N.A. Algarou, Y. Slimani, A. Sadaqat, A. Baykal, A. Manikandan, S.V. Trukhanov, A.V. Trukhanov, I. Ercan, Investigation of exchange coupling and microwave properties of hard/soft (SrNi<sub>0.02</sub>Zr<sub>0.01</sub>Fe<sub>11.96</sub>O<sub>19</sub>)/(CoFe<sub>2</sub>O<sub>4</sub>)<sub>x</sub> nanocomposites, Materials Today Nano, 18 (2022) 100186.
27. M. P. Mani, A.A.M. Faudzi, S. Mohamaddan, A. F. Ismail, R. Rajasekar, A. Manikandan, S. K. Jaganathan, Grapefruit oil and cobalt nitrate loaded polyurethane hybrid nanofibrous scaffold for biomedical applications, Frontiers in Materials Biomaterials, 9 (2022) 827009.
28. S. A. Al-Zahrani, A. Manikandan, K. Thanrasu , A. Dinesh, K. K. Raja, M.A. Almessiere, Y. Slimani, A. Baykal, S. Bhuminathan, S. R. Jayesh, J. Ahmed, H. S. Alorfi, M. A. Hussein, I. Khan, A. Khan, Influence of Ce<sup>3+</sup> on the structural, morphological, magnetic, photocatalytic and antibacterial properties of spinel MnFe<sub>2</sub>O<sub>4</sub> nanocrystals prepared by combustion route, Crystals, 12 (2022) 268.
29. B. Unal, M. A. Almessiere, A. V. Trukhanov, A. Baykal, Y. Slimani, M. V. Silibin, A. Ul-Hamid, A. Manikandan, A study on the conductivity, dielectric, and microwave properties of (SrNb<sub>x</sub>Y<sub>x</sub>Fe<sub>12-2x</sub>O<sub>19</sub> (0.00 ≤ x ≤ 0.05) nanohexaferrites, Journal of Materials Research and Technology, 17 (2022) 2975-2986.
30. B. A. Kumar, V. Vetrivelan, G. Ramalingam, A. Manikandan, S. Viswanathan, P. Boom, G. Ravi, Computational studies and experimental fabrication of DSSC device assembly on 2D-layered TiO<sub>2</sub> and MoS<sub>2</sub>@TiO<sub>2</sub> nanomaterials, Physica B: Condensed Matter, 633 (2022) 413770.

31. T.L. Ajeesha, A. Manikandan, A. Ashwini, Sagaya Jansi, M. Durka, M. A. Almessiere, Y. Slimani, A. Baykal, A. M. Asiri, H. A. Kasmery, A. Khan, A.A.P. Khan, P. Madhu, M. George, Structural investigation of Cu doped calcium ferrite ( $\text{Ca}_{1-x}\text{Cu}_x\text{Fe}_2\text{O}_4$ ;  $x = 0, 0.2, 0.4, 0.6, 0.8, 1$ ) nanomaterials prepared by co-precipitation method, *Journal of Materials Research and Technology*, 18 (2022) 705-719.
32. M. Sertkol, S. Güner, M. A. Almessiere, Y. Slimani, A. Baykal, H. Gungunes, E. M. Alsulami, F. Alahmari, M. A. Gondal, S. E. Shirasath, A. Manikandan, Effect of  $\text{Bi}^{3+}$  ions substitution on the structure, morphology, and magnetic properties of Co-Ni spinel ferrite nanofibers, *Materials Chemistry and Physics*, 284 (2022) 126071.
33. A. Dinesh, K. Kanmani Raja, A. Manikandan, M. A. Almessiere, Y. Slimani, A. Baykal, H. S. Alorfi, M. A. Hussein, A. Khan, Sol-gel combustion synthesis and photocatalytic dye degradation studies of rare earth element Ce substituted Mn-Zn ferrite nanoparticles, *Journal of Materials Research and Technology*, 18 (2022) 5280-5289,
34. Y. Slimani, M. A. Almessiere, A. D. Korkmaz, A. Baykal, A. Manikandan, H. Gungunes, M. S. Toprak, Ultrasound-assisted synthesis and magnetic investigations of  $\text{Ni}_{0.4}\text{Cu}_{0.4}\text{Zn}_{0.2}\text{Ga}_x\text{Gd}_x\text{Fe}_{2-2x}\text{O}_4$  ( $0.00 \leq x \leq 0.04$ ) nanosized spinel ferrites, *Applied Physics A* 128 (2022) 1-14.
35. M. Sertkol, Y. Slimani, M.A. Almessiere, H. Sozeri, R. Jermy, A. Manikandan, S.E. Shirasath, A. UI-Hamid, A. Baykal, Sonochemical synthesis of  $\text{Mn}_{0.5}\text{Zn}_{0.5}\text{Er}_x\text{Dy}_x\text{Fe}_{2-2x}\text{O}_4$  ( $x \leq 0.1$ ) spinel nanoferrites: Magnetic and textural investigation, *Journal of Molecular Structure*, 1258 (2022) 132680.
36. M. P. Mani, A. A. M. Faudzi, S. Mohamaddan, A. F. Ismail, R. Rathanasamy, A. Manikandan, S. K. Jaganathan, Engineered polymer matrix novel biocompatible materials decorated with eucalyptus oil and zinc nitrate with superior mechanical and bone forming abilities, *Arabian Journal of Chemistry*, 104079 (2022).
37. M. A. Almessiere, S. Güner, Y. Slimani, A. Baykal, S. E. Shirasath, A. D. Korkmaz, R. Badar, A. Manikandan, Investigation on the structural, optical, and magnetic features of  $\text{Dy}^{3+}$  and  $\text{Y}^{3+}$  co-doped  $\text{Mn}_{0.5}\text{Zn}_{0.5}\text{Fe}_2\text{O}_4$  spinel ferrite nanoparticles, *Journal of Molecular Structure* 1248, 131412 (2022).

38. H. Tombuloglu, N. Albenayyan, Y. Slimani, S. Akhtar, G. Tombuloglu, M. Almessiere, A. Baykal, I. Ercan, H. Sabit, A. Manikandan, Fate and impact of maghemite ( $\gamma$ -Fe<sub>2</sub>O<sub>3</sub>) and magnetite (Fe<sub>3</sub>O<sub>4</sub>) nanoparticles in barley (*Hordeum vulgare L.*), Environmental Science and Pollution Research, 29 (3), 4710-4721.
39. A. Alagarsamy, S. Chandrasekaran, A. Manikandan, Green synthesis and characterization studies of biogenic zirconium oxide (ZrO<sub>2</sub>) nanoparticles for adsorptive removal of methylene blue dye, Journal of Molecular Structure, 1247 (2022) 131275.
40. M. P. Mani, A. A. M. Faudzi, S. Mohamaddan, A. F. Ismail, R. Rathanasamy, A. Manikandan, S. K.Jaganathan, Engineered polymer matrix novel biocompatible materials decorated with eucalyptus oil and zinc nitrate with superior mechanical and bone forming abilities, Arabian Journal of Chemistry, 15, 2022, 104079.
41. M. A. Almessiere, Y. Slimani, S. Ali, A. Baykal, R. J. Balasamy, S. Guner, İ. A Auwal, A. V Trukhanov, S. V. Trukhanov, A. Manikandan, Impact of Ga<sup>3+</sup> Ions on the Structure, Magnetic, and Optical Features of Co-Ni Nanostructured Spinel Ferrite Microspheres, Nanomaterials, 2022, 12(16), 2872.
42. A. Khan, A. A. P. Khan, H. M. Marwani, M. M. Alotaibi, A. M. Asiri, A. Manikandan, S. Siengchin, S. M. Rangappa, Sensitive Non-Enzymatic Glucose Electrochemical Sensor Based on Electrochemically Synthesized PANI/Bimetallic Oxide Composite, Polymers, 2022, 14(15), 3047.